Research Square

Preprints are preliminary reports that have not undergone peer review.
They should not be considered conclusive, used to inform clinical practice,
or referenced by the media as validated information.

Optimized Mg doped ZnO Thin Film Sensors for Breath Acetone Biomarker Detection

Mangesh Awale
Dayanand Science College
Lahu Kathwate
Dayanand Science College
Vaishali Chandak
Dayanand Science College
Shweta Lokhande
shweta.lokhande266488@gmail.com
Dayanand Science College

Research Article

Keywords: Breath biomarker, Gas sensor, Nanostructures, Non-invasive diagnostics

Posted Date: May 25th, 2026

DOI: https://doi.org/10.21203/rs.3.rs-9343032/v1

License: This work is licensed under a Creative Commons Attribution 4.0 International License.
Read Full License

Additional Declarations: No competing interests reported.

Optimized Mg doped ZnO Thin Film Sensors for Breath Acetone Biomarker Detection

M. B. Awale[b], L. H. Kathwate[a], V. S. Chandak[a], S. D. Lokhande[a]*

[a]Thin Films and Materials Science Research Laboratory, Department of Physics, Dayanand Science College, Latur – 413512, Maharashtra, India.

[b]Department of Physics, Jawahar Arts, Science and Commerce College, Andur, Tuljapur, Osmanabad, 413603, Maharashtra, India.

*Corresponding authors email id: shweta.lokhande266488@gmail.com,

Tel: +91-2382-221149; Fax+91-2382-221149

Abstract

Acetone in exhaled breath is an important biomarker linked to diabetes, liver dysfunction and metabolic disorders. Breath analysis offers a painless and continuous alternative to invasive blood-based diagnostics. However, challenges remain in achieving reliable detection at low concentrations and room temperature. While ZnO is widely studied as a sensing material, reports on Mg-doped ZnO for breath-acetone detection are rare. Mg-doped ZnO thin films were synthesized by spray pyrolysis with different doping levels. Structural, morphological, elemental and optical properties were analyzed, and acetone sensing performance was evaluated at room temperature and low ppm concentrations. This study demonstrates that Mg doping can effectively tune ZnO thin films for acetone sensing, but the doping level is critical. At lower Mg concentration, films exhibited improved crystallinity, favorable surface morphology and superior sensing response with fast kinetics at low ppm levels. In contrast, higher Mg content reduced the density of active sites and diminished sensing performance. By highlighting both the potential and the limitations of Mg incorporation, this work addresses an underexplored area in gas sensor research and provides insights for developing room-temperature, low-power non-invasive acetone breath analyzers.

Keywords: Breath biomarker; Gas sensor; Nanostructures; Non-invasive diagnostics.

1. Introduction

The monitoring of volatile organic compounds (VOCs), especially acetone, is crucial because it acts both as a harmful environmental pollutant and an important biomarker for non-invasive medical diagnostics. Prolonged exposure to acetone, even at concentrations near 173 ppm, can cause respiratory issues and neurotoxic effects. In breath analysis, acetone levels above approximately 1.8 ppm are often linked to diabetes [1]. Excess ketone bodies can cause severe dehydration, acid–base imbalance, hypotension and in extreme cases, coma or death. In healthy individuals, breath acetone typically ranges from 0.3 to 0.9 ppm, even during fasting or ketogenic diets. For diabetic patients, acetone monitoring is vital for detecting and managing diabetic ketoacidosis [2]. Moreover, acetone is highly volatile and easier to detect than many other breath biomarkers. Its strong link to diabetes function makes it especially important for early diagnosis using breath-based sensors [3]. This can support in evaluating the effectiveness of treatment in patients with lever diseases [4]. Moreover, as technology develops in material science, gas sensors are expected to play a significant role in various areas such as energy-efficient smart homes and maintaining atmosphere balance [5]. Room temperature sensing of acetone is particularly important due to its widespread industrial use in agriculture, food processing and pharmaceuticals and because it enables more practical operation without the need for external heating [6,7].

ZnO thin films have been extensively studied for gas sensing because of their high sensitivity and rapid response [8]. The gas sensing mechanism of ZnO involves the adsorption and desorption of gas molecules on the film surface which alters the electrical resistance of the sensor [9]. This process is influenced by the film's microstructure, crystallinity and surface-to-volume ratio [10]. Achieving optimal sensing performance at room temperature is highly desirable as it reduces the energy consumption and complexity of the sensing system. Uniqueness in optical and electrical properties makes ZnO an emerging metal oxide. Transparent conducting oxides, LEDs, gas sensors and flat panel displays are some of the

technological applications of ZnO [11-13]. ZnO has a direct band gap of 3.37 eV with a large exciton binding energy of 60 meV [14]. ZnO is an n-type semiconductor material. Research indicates that by adjusting the temperatures, the resistivity values of ZnO films can be maintained between 10^{-3} Ω.m and 10^{-4} Ω.m [15]. ZnO has a wurtzite structure which belongs to the space group P_6m_3c [16]. The wurtzite structure is a hexagonal lattice in which each Zn^{2+} ion is tetrahedrally bonded to four O^{2-} ions. In recent years, ZnO has gained importance due to its stable physical and chemical properties, non-toxic nature and excellent optical and electrical properties. All these interesting properties and applications of ZnO have attracted many researchers to study it in thin film form.

The properties of the prepared films are influenced by various parameters, including the concentration of the precursor, type of substrate, substrate temperature, carrier gas pressure and doping effect [17-19]. Recent research has highlighted the significant impact of doping on the properties of metal oxide thin films [20-22]. Specific dopant can affect the droplet size of the precursor solution, deposition rate, microstructure and morphology of the films. However, pure ZnO as a sensing material show drawbacks such as high operating temperature, limited detection capability, low selectivity and prolonged response and recovery times. Introducing suitable dopants into ZnO is an effective approach to enhance its gas sensing performance [23]. Improved interfacial charge transport and solid-state diffusion play a crucial role in enhancing gas sensing performance. Mg is considered a promising dopant for ZnO due to its natural abundance, non-toxic nature, stability and divalent state which help overcome certain limitations observed with other dopants [24].

Furthermore, the gas sensing properties of ZnO thin films are highly dependent on their microstructure and surface morphology which are influenced by doping [25-27]. Enhanced crystallinity and increased surface to volume ratio can improve gas adsorption and desorption processes, thereby enhancing the sensitivity and response time of the gas sensors. Additionally, increased defect densities can lead to more stable and reliable sensor performance. However,

when ZnO is overloaded with Mg dopant, it can trigger excessive densification and the emergence of secondary phases (e.g., MgO) which in turn diminish surface porosity and reduce the number of active adsorption sites [28]. Therefore, maintaining an optimal Mg concentration within the ZnO matrix is essential to achieve superior sensing performance. In electrochemically deposited Mg-doped ZnO thin films, carrier (donor) density increases significantly with rising Mg content from about 1.23×10^{20} cm^{-3} in undoped ZnO up to around 7.24×10^{20} cm^{-3} at higher Mg levels [29]. Recent studies were carried out using UV-enhanced Mg-doped MOF-ZnO sensor for n-butanol gas detection at lower temperatures. It showed Mg-modified ZnO from MOF precursor which improved low-temp gas response under UV [30].

The thin films deposition technology has significantly improved over the past few years which depends primarily on the demand for new products and devices in the electronics, optical and healthcare industries. There are several physical and chemical methods available for ZnO thin films synthesis, such as pulsed laser deposition, magnetron sputtering, chemical vapor deposition, molecular beam epitaxy, hydrothermal, sol–gel coating, SILAR method, chemical bath deposition and spray pyrolysis [31-36].

Among these methods, spray pyrolysis stands out due to its simplicity, cost-effectiveness and time-saving nature. Moreover, the spray pyrolysis technique provides full control over the film thickness and uniformity. The specific effect Mg doping on ZnO thin films prepared by spray pyrolysis have been less extensively studied. Also, since gas sensing is a surface-dependent phenomenon, controlling the surface morphology is crucial. This can be effectively achieved by regulating dopant concentration. Breath acetone monitoring serves as a non-invasive diagnostic tool, as elevated levels are often linked to liver dysfunction or metabolic disorders. Detecting acetone in exhaled breath helps early diagnosis and continuous monitoring without the need for invasive blood sampling. Therefore, our aim in this paper is to investigate the doping effect for influencing the properties of ZnO thin films including their breath analysing capabilities. In this study, we systematically examine the structural, optical

and gas sensing properties of Mg doped ZnO thin films. The gas sensing study of pure ZnO thin films were already investigated in our previous study [37]. Understanding Mg doping effect is crucial for optimizing the deposition process and enhancing the performance of ZnO-based devices especially for gas sensing in breath analysis and biomarker detection.

2. Materials and Methods

0.1M Zinc acetate dihydrate ($Zn(CH_3COO)_2 \cdot 2H_2O$) and 0.1M of Magnesium acetate dehydrate [$Mg(CH_3COO)_2 \cdot 2H_2O$] of 99% purity was used as precursors to obtain Mg doped ZnO thin films. Distilled water was used as a solvent. To ensure complete dissolution, resulting solution was stirred for 10 minutes using a magnetic stirrer. The spray pyrolysis technique was employed for the deposition of ZnO thin films. Cleaned glass substrates were preheated to 400°C before deposition. The prepared solution was added to the reservoir of the spray pyrolysis equipment which allowed it to flow through the nozzle. The deposition was carried out at three Mg dopant concentrations 2%, 4% and 6% with compressed air maintained 30 psi during deposition to prevent rapid cooling of the substrates. The nozzle-to-substrate distance was 20 cm, flow rate was 2 ml/min and the deposition time was 10 minutes. After deposition, the substrates were allowed to cool and their thicknesses were measured using the weight difference method with a digital weight balance. The schematics of spray pyrolysis set-up is shown in fig. 1.

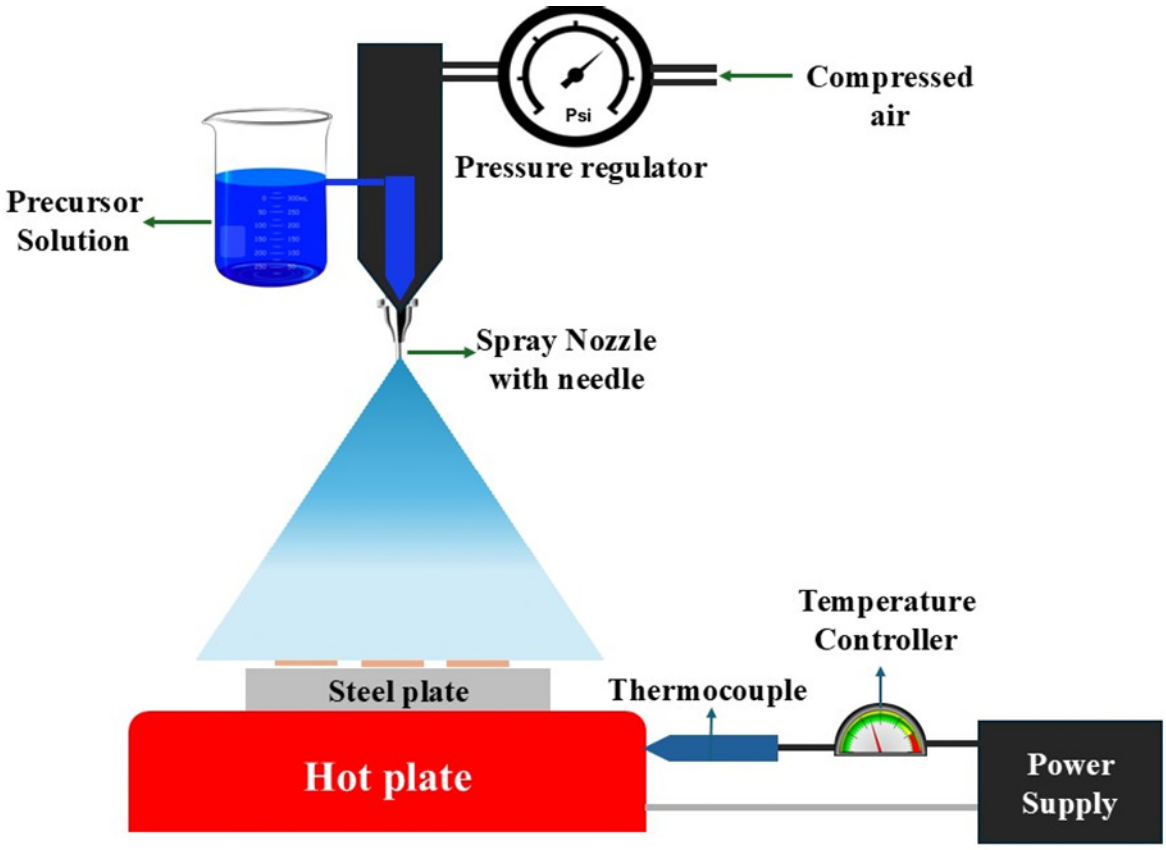


Fig. 1. Schematics of spray pyrolysis set-up.

3. Characterization of deposited thin films

The thickness of the prepared samples was maintained for 550 to 600 nm by regulating the spray rate time keeping all the parameters constant. X-ray diffraction spectra of the prepared thin film samples were recorded using Panalytical Empyrean X-ray Diffractometer system using $CuK_{\alpha 1}$ (λ=1.5406 Å) for 2θ values ranging from 20-80^{o}. The optical absorption and transmission properties of films were studied using Shimadzu 1900i-UV–VIS spectrophotometer in the wavelength range of 300 nm to 1100 nm. Morphology of the prepared thin-film samples was analysed using FEI Nova Nano SEM 450. Elemental contents were studied using Pegasus EDS-EBSD system. Furthermore, prepared thin film samples were studied for acetone gas sensing ability at room temperature using laboratory-built microcontroller-based gas sensing set-up connected to Keithley electrometer 6517B.

4. Result and Discussion

4.1. Structural Studies

Synthesized thin films are analysed using X-ray Diffractometer. Intensity verses 2θ variation is observed for Mg doped ZnO thin films samples (Fig. 2). From the graph it has been observed that diffraction peaks belong to hexagonal wurtzite ZnO structure. By calculating the FWHM, average crystallite size values of the (1 0 0), (0 0 2), (1 0 1), (1 0 2), (1 1 0), (1 0 3) and (1 1 2) peaks have been evaluated using equation (1)[38]:

$$D = \frac{K\lambda}{\beta \cos\theta} \tag{1}$$

where K is the Scherrer's constant, λ is the wavelength of X-ray beam, $\beta\ is$ the full width half maximum of the diffraction peak, θ is the angle of diffraction peak. Undoped ZnO samples structural parameters were already reported in our previous literature [37]. It is observed that grain size increases form around 19 to 23 nm with increasing dopant concentration from 2% to 6%. The growth and coalescence of crystallites can be made easier by increased surface mobility which may leads to a larger average crystallite size [39]. Similar results were also reported by S. Hameed et. al. [40]. For calculation of lattice parameters 'a' and 'c' the following hexagonal phase formula was used [41].

$$\frac{1}{d^2_{(h,k,l)}} = \frac{4(h^2 + hk + k^2)}{3a^2} + \frac{l^2}{c^2} \tag{2}$$

where, $d_{h,k,l}$ is an interplanar spacing distance, $h, k\ and\ l$ are miller indices, a and c are lattice parameters. It can be observed that (002) peak is most intense peak indicating an extensive orientation along c-axis. The corresponding lattice constant value of 2% Mg films is closely matched with the standard values. Initially, lattice constant value decreases and later increases slightly for 6% Mg. Not only that but the intensity of (002) plane initially increases with increase in doping as shown in fig. (2) for 2% and 4% indicating that film crystallinity is

enhanced for lower doping which may be due to lower compressive stress present at. Later, as the doping increased to 6% the intensity is found to be considerably decreased which may be due to inefficiency of solute particle to get adsorbed on the surface at Mg doping and degrading the crystallinity. H. Heryanto [42], observed that as the Mg concentration increased there was a decrease in the intensity of XRD peaks and peak shifted to lower angles. Their analysis revealed that while ZnO remained the dominant phase, Mg-doped samples exhibited additional peaks corresponding to MgO and minor metallic Mg. These secondary phases indicate incomplete substitution of Zn^{2+} by Mg^{2+} which leads to structural impurities. Such extra peaks reflect lattice strain, defects and altered d-spacing which can negatively affect the material's sensing performance. The dislocation density (δ) and micro strain (ε) values are estimated using equations [43],

$$\delta = \frac{1}{D^2} \tag{3}$$

$$\varepsilon = \frac{c_{film} - c_0}{c_o} \tag{4}$$

where c_{film} indicates an obtained lattice parameter value from the XRD and c_o indicates the standard ZnO lattice parameter value (c_o= 5.204Å). The dislocation density decreases as expected as it is inverse of crystallite size with increase in doping [44]. The strain values at first decreases when Mg concentration increased from 2% to 4% but slightly increases for 6% Mg as shown in table (1). This variation in microstrain again indicating the enhancement in the crystallinity of the film for lower doping values and reduction in crystallinity for higher doping (6%Mg) as mentioned above. The volume of the crystallites can be determined by [45],

$$V = \frac{\sqrt{3}}{2} a^2 c \tag{5}$$

The variation in volume of the unit cell is consistent with variation in lattice parameter values. The volume of the unit cell is observed to fluctuate slightly with doping. For 2% Mg the volume is 47.6829 Å³, which decreases to 47.3872 Å³ for 4% Mg doping. This slight reduction could be attributed to the denser packing of grains. However, for 6% Mg, the volume increases again to 47.6330 Å³ which may suggest the growth of larger grains or slight relaxation in the crystal lattice.

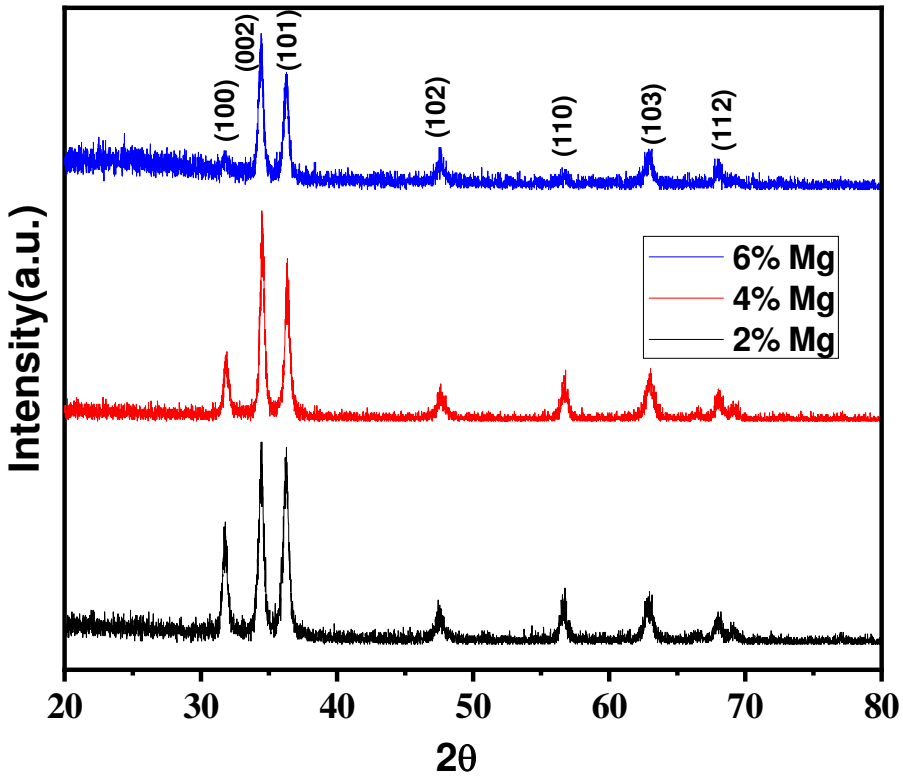


Fig. 2. XRD patterns of ZnO films for 2%, 4% and 6% Mg doping.

Table 1. Structural parameters of ZnO thin films.

Mg Doping (%)	a (Å)	c (Å)	c/a	D (nm)	Strain	Volume $(Å)^3$	u	δ (lines/nm^2)
2	3.2522	5.2089	1.6016	19.58	0.004372	47.6829	0.3798	0.002608
4	3.2446	5.1965	1.6015	22.94	0.003793	47.3872	0.3799	0.001899
6	3.2539	5.2088	1.6030	23.34	0.003916	47.6330	0.3797	0.001834

4.2. Optical Studies

Optical properties of deposited films with Mg doping were measured by using UV-VIS spectrophotometer carried out from 350 nm to 1100 nm in both transmittance and absorption mode as shown in fig. 3 and fig. 4. From transmittance curve it can be observed that all the thin films have good transmittance from 50 to 90% which is required for many optoelectronics and solar cell applications. As Mg doping increasing from 2% to 6%, the transmittance is observed to be decreased from wavelength range of 400 nm to 600 nm [46]. The maximum transmittance is observed for 2% Mg around 90% for visible range. Small fluctuation in the transmittance observed may be due to the interference in the thin films.

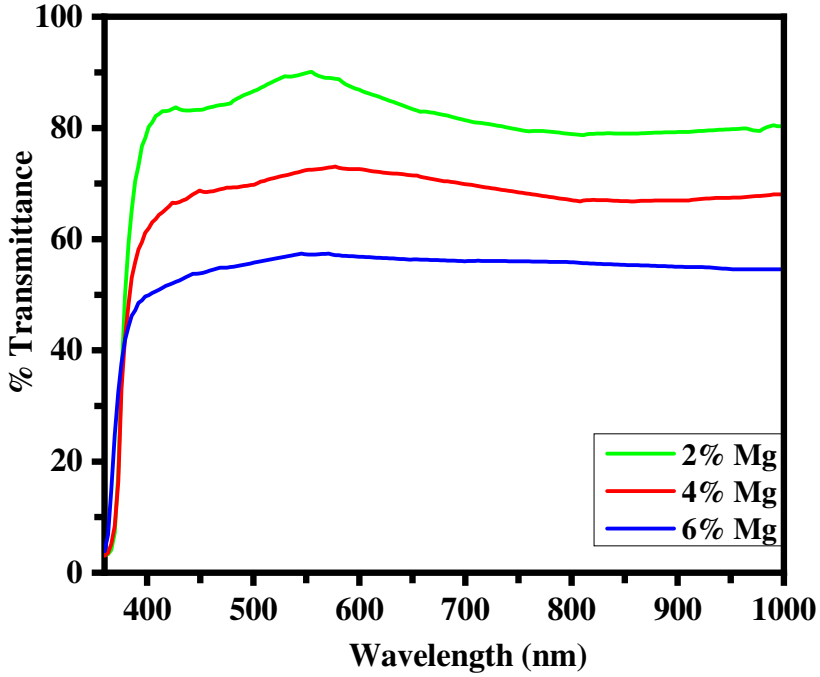


Fig. 3. Transmittance spectra of ZnO films for 0%, 2% and 4% Mg.

Fig. 4. shows the variation of absorption with wavelength for three depositions. Optical band gap was determined by the absorbance spectra. Coefficient of absorbance is given by the relation [47],

$$(\alpha h\nu)^2 = A(h\nu - E_g) \tag{6}$$

where E_g is energy gap, hυ is photon energy, A is constant and n depends on the type of optical transition involved. The values of 'n' are 1/2, 2, 3/2 and 3 which belongs to allowed direct, allowed indirect, forbidden direct and forbidden indirect transitions respectively. The UV absorption spectrum of ZnO thin films shows that minimum absorption seen at 2% Mg and the strong absorbance is observed at 6% Mg in the visible region of spectrum for ZnO thin films. Strong absorbance may be due to the fact that incoming photons have enough energy for excitation of electrons from valance band to conduction band [48].

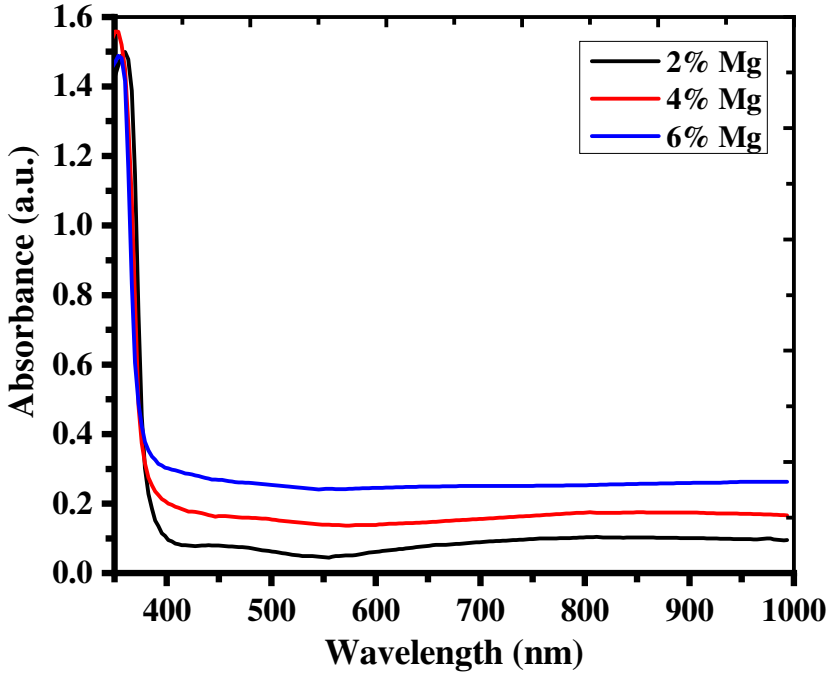


Fig. 4. Absorbance spectra of ZnO films for 0%, 2% and 4% Mg doping.

The energy band gap for the direct band gap material was determined based on the analysis of the absorption spectra. Fig. 5 shows an increase in energy band gap values with an increase in Mg doping. Similar results were reported earlier [49]. Energy band gap values for different Mg doping are given in table 2. It is observed that with increase in Mg doping the band gap increases. Changes in crystallite size and reduced strain in the film at higher doping may further influence the electronic structure which leads to an increase in the band gap. H. Ennaceri et al. [50], explored the influence of stress on properties of sprayed ZnO thin films and mentioned that the energy band gap increases with both compressive strain and tensile stress. This increase is attributed to the alterations in inter-atomic spacing along the c-axis which affects the overlap of atomic orbitals and the band structure.

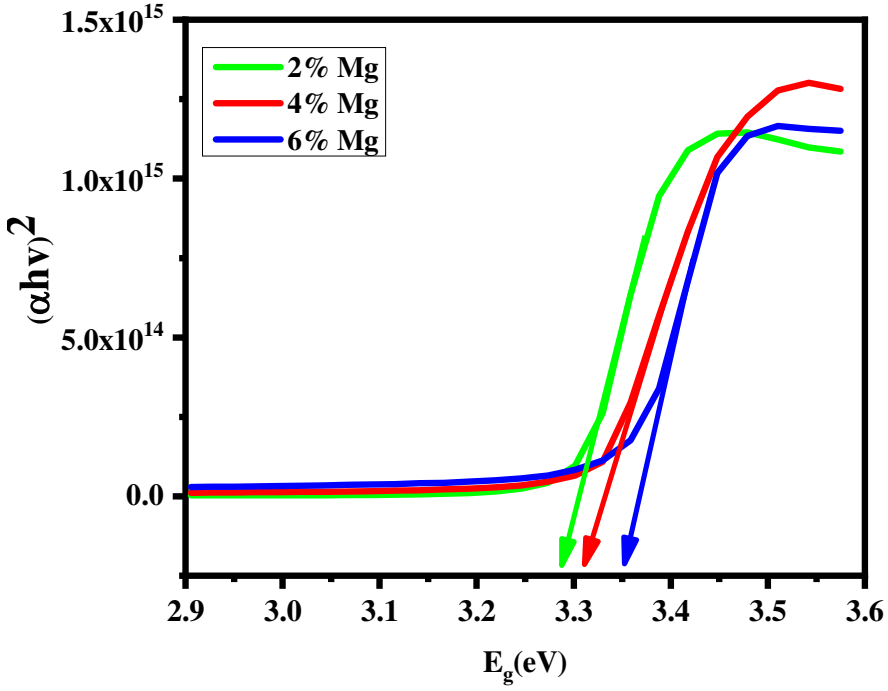


Fig. 5. Energy band gap spectra of ZnO films for 2%, 4% and 6% Mg doping.

Table 2. Variation in Energy band gap with Mg doping.

Mg doping (%)	Bandgap (eV)
2	3.28
4	3.31
6	3.34

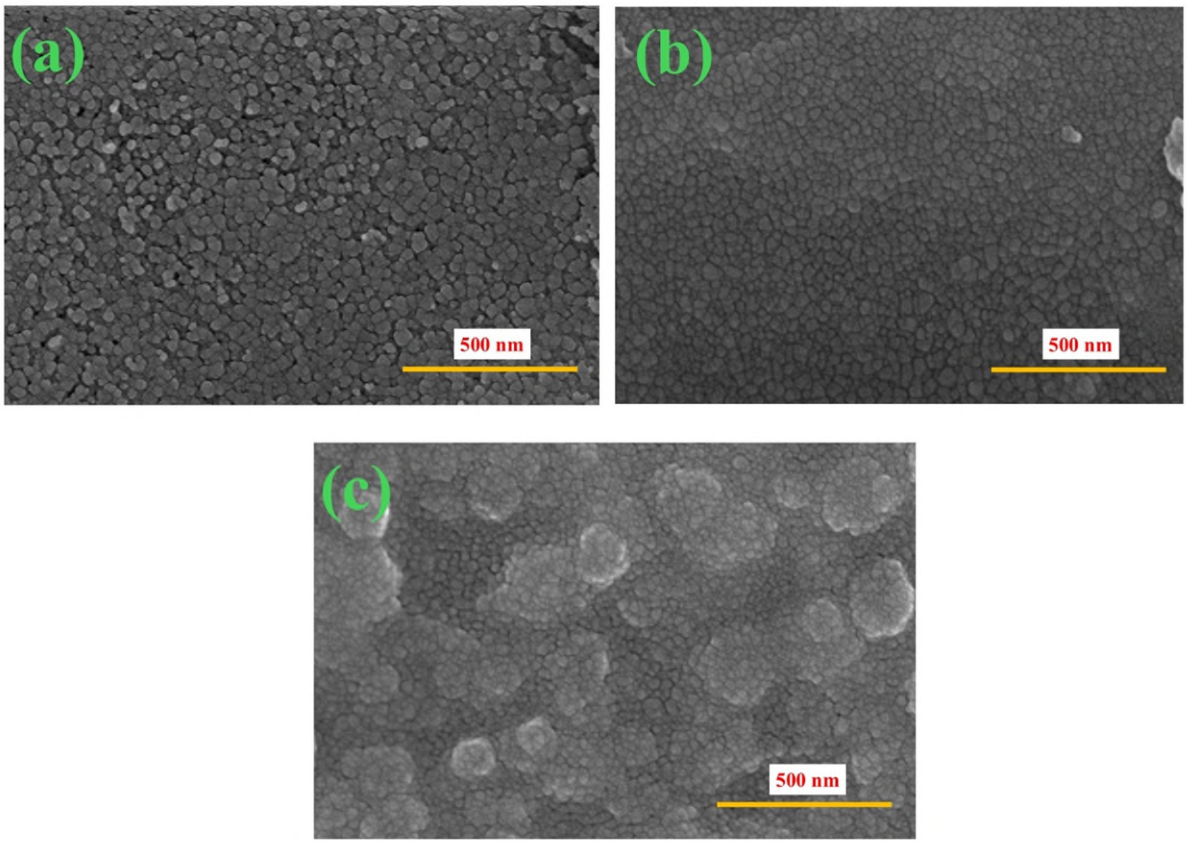


Fig. 6. FESEM images of a) 2% Mg, b) 4% Mg and c) and 6% Mg doping.

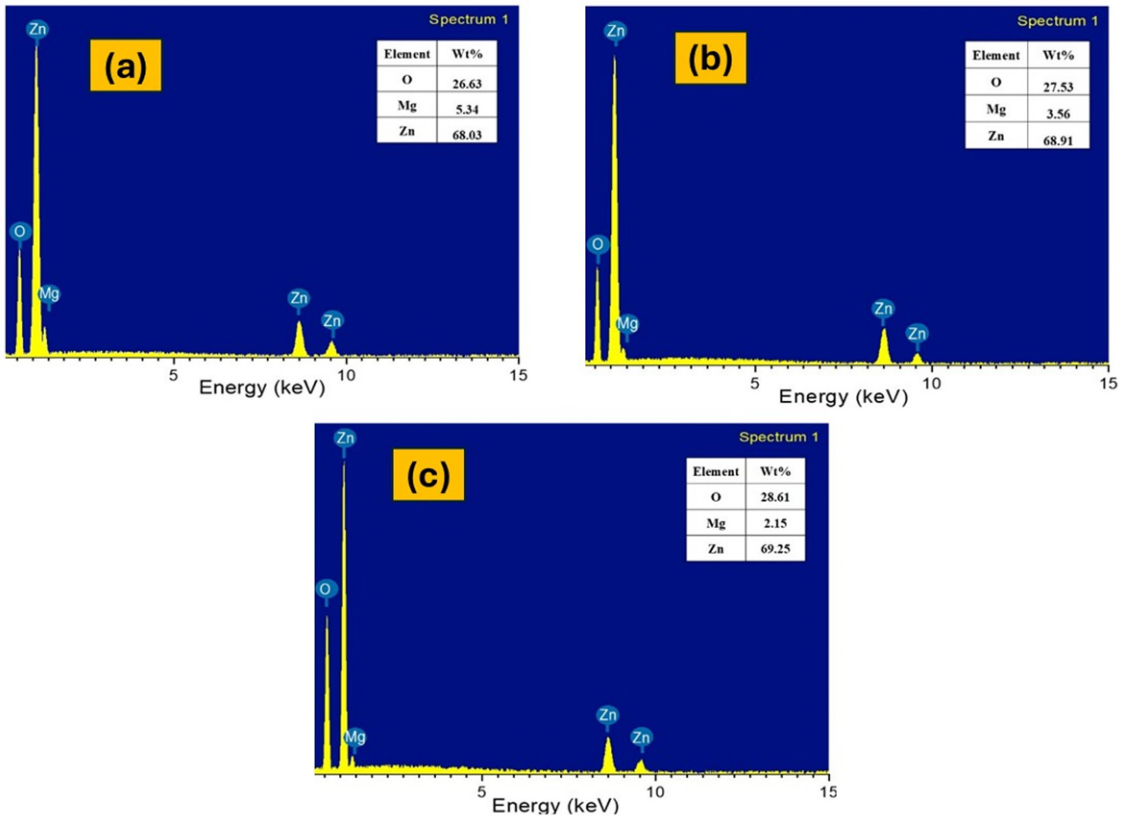


Fig. 7. EDX spectras of a) 2% Mg, b) 4% Mg and c) and 6% Mg doping.

FESEM analysis revealed a polycrystalline structure for all ZnO films with visible grain boundaries. The grain morphology was observed to evolve with increasing doping. Grain appears granular and rounded. Fig. 6(a) indicates that the surface consists of densely packed, small and spherical grains indicating a relatively smooth and uniform morphology at 2% Mg. Grain boundaries are clearly visible and the distribution appears homogeneous. Fig. 6(b) shows densely packed grains but with fewer distinct boundaries compared to films deposited at 2% Mg [Fig. 6 (a)], implying a more compact structure. Higher doping led to larger grain sizes, likely due to enhanced atomic diffusion during growth, which promotes grain coalescence and reduces grain boundary density. Consequently, this leads to the formation of larger grains during deposition [Fig. 6 (b)]. The compact structure may result in slightly lower surface area and fewer diffusion pathways for gas molecules. Further, 6% Mg doping, grains become larger and more distinct [Fig. 6 (c)]. Samples exhibit a highly dense morphology with clusters of

granules. This more compact and dense structure reduces the porosity and limits the diffusion of gas molecules to the active sensing sites. The dense structure suggests a more durable but less responsive sensor due to the decreased surface-to-volume ratio. Eslamian et al. [51] studied the influence of precursor and pressure on the morphology and crystallinity of nanostructures prepared by spray pyrolysis. Their results highlighted that even at low pressures, an adequate air motion could disperse the droplets effectively and minimizes collisions. This controlled dispersion resulted in uniform particle morphology and contributed to improved crystallinity and stability of the deposited materials. Elemental analysis of the prepared samples with increasing Mg content was performed to determine the specific elemental composition of the materials and confirmed the successful incorporation of Mg as shown in Fig. 8. The results for undoped ZnO samples have been reported earlier [37].

4.4. Gas sensing study

Breath analysis offers a non-invasive approach for diagnosing various diseases by detecting specific VOCs and gases such as ammonia, nitric oxide and acetone. These biomarkers are linked to conditions like kidney dysfunction, asthma and diabetes. However, their detection at trace levels demands high-performance gas sensor. Volatile biomarkers present in exhaled breath have been linked to specific diseases and metabolic disorders as shown in table 4. Optimizing dopant levels during the fabrication of gas sensors is crucial for enhancing the surface area and improving sensing capabilities [52]. A well-optimized, parameters can lead to a more porous structure with a larger surface area which is beneficial for gas adsorption. The increased surface area provides more active sites for gas molecules to interact which results in improved sensitivity and faster response times in gas detection [53].

Gas sensing is a surface-driven process that relies on the interaction between gas molecules and the sensing material. This interaction typically occurs through the adsorption and desorption of gas molecules (oxygen species) on the surface of the material. When oxygen

molecules from the surrounding air come into contact with the surface of the sensing material, they adsorb onto it and form adsorbed oxygen species such as O^-, O_2^- and O^{2-}. Surface reaction is mentioned below [54]:

$$O_{2(gas)} \rightarrow O_{2(ads)}$$
$$O_{2(ads)} + e^- \rightarrow O^-_{2(ads)}$$
$$O^-_{2(ads)} + e^- \rightarrow 2O^-_{(ads)}$$
$$2O^-_{(ads)} + e^- \rightarrow O^{2-}_{(ads)}$$

These adsorbed species act as active sites for further interaction with target gas molecules. During the gas sensing process, target gas molecules interact with these adsorbed oxygen species undergoes a chemical reaction or charge transfer. This interaction alters the concentration of adsorbed oxygen species on the surface resulting in a change in the electrical resistance of the sensing material. The efficiency and sensitivity of this process are highly dependent on the available surface area and the number of active sites for gas adsorption. Moreover, the adsorption and desorption processes are dynamic and reversible, allowing the sensor to recover its baseline properties once the target gas is removed. This reversible nature of gas adsorption and desorption is crucial for repeated and reliable gas detection. A larger surface area not only increases the number of active sites for adsorption but also facilitates the rapid desorption of gas molecules that contributes to faster response and recovery times in gas sensing applications. The gas sensing was analysed for 5 ppm acetone at room temperature using ZnO thin films. Fig. 8 (a, b and c) indicates response curves (resistance vs time curves) of ZnO thin films at doping 2%, 4% and 6% respectively. Acetone sensing response for all the films were evaluated using response formula [55],

$$S\% = \frac{R_a - R_g}{R_a} \times 100 \tag{7}$$

where S indicates gas response, R_a indicates resistance of the films in air and R_g indicates resistance of the films in presence of target gas. The sensors performance was evaluated under varying dopant levels with results summarized in Table 3**.** For 2% Mg, sensor exhibited the highest response of 88% with a rapid response time of 12 seconds and a recovery time of 11 seconds which indicates efficient gas detection and swift recovery. As the Mg doping concentration increased to 4% and 6%, response decreased to 78% and 75% respectively. Concurrently, the response time increased to 18 seconds at 30 psi and 24 seconds at 6% Mg. While the recovery time also extended to 20 seconds and 22 seconds respectively. This trend suggests that higher Mg doping may hinder the sensor's ability to detect gas quickly and recover to its baseline state due to reduced gas interaction or slower diffusion rates at elevated Mg concentration. Thus, the sensor shows optimal performance at lower doping which makes it more suitable for applications requiring fast detection and recovery times.

Table 3. Effect of Mg doping on gas sensor response, response time and recovery time.

Mg doping (%)	**Response (%)**	**Response time (s)**	**Recovery time (s)**
2	88	12	11
4	78	18	20
6	75	24	22

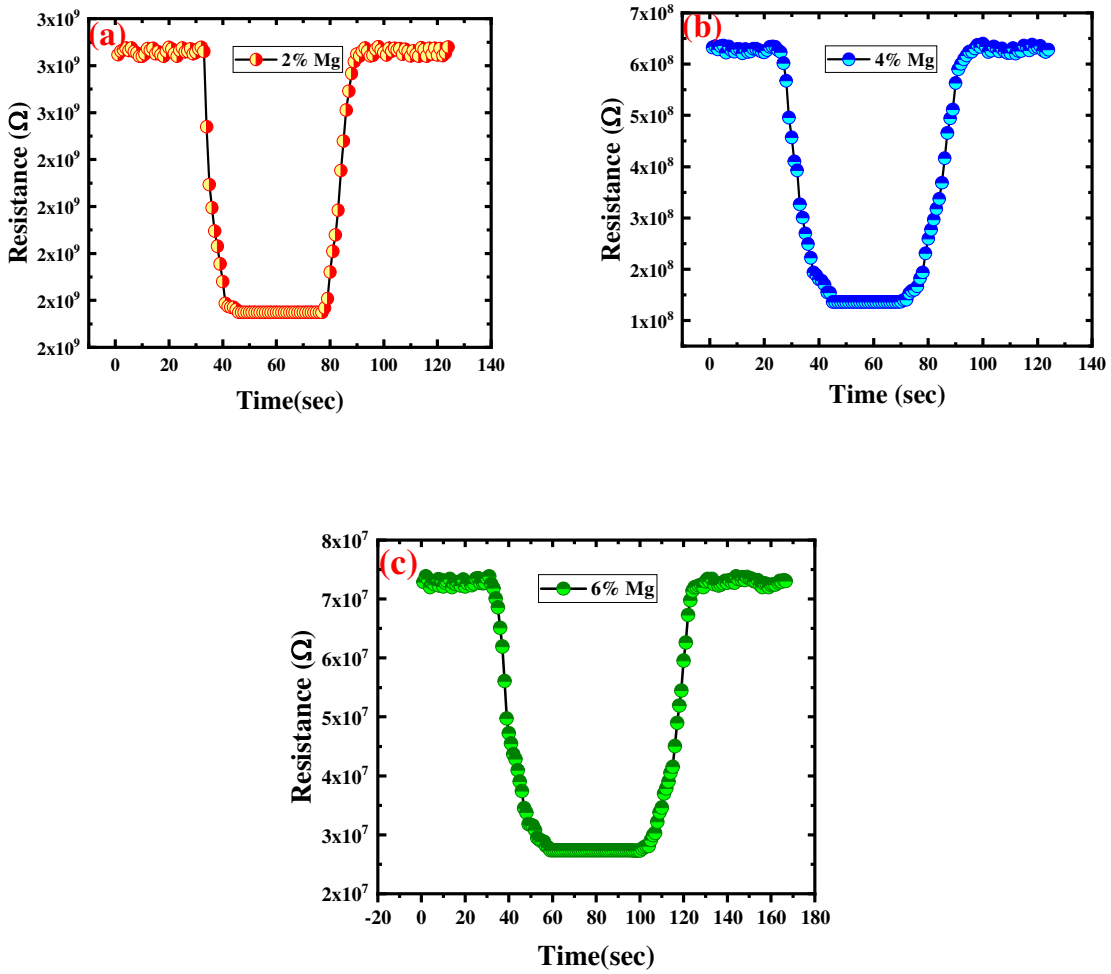


Fig. 8. Response curves of ZnO films for 2%, 4% and 6% Mg doping.

Table 4. Common breath gas biomarkers, their associated diseases and diagnostic roles

Breath Gas (Biomarker)	Associated Disease / Condition	Diagnostic Role	Ref.
Ammonia	Kidney disease, Helicobacter pylori germ infection, liver disease	Indicates impaired renal function and urea breakdown	[56]
Nitric Oxide	Asthma, chronic obstructive pulmonary disease, airway inflammation	For airway inflammation	[57]
Carbon Monoxide	Oxidative stress, smoking, hemolytic disorders	Elevated in smokers and inflammation	[58]
Hydrogen Sulphide	Gastrointestinal disorders, bacterial overgrowth, halitosis	Byproduct of sulfur-reducing bacteria	[59]
Methane	Constipation, irritable bowel syndrome	Linked to intestinal methanogen overgrowth	[60]
Acetone	Diabetes, ketogenic diet, prolonged fasting	Endogenous from fat metabolism	[61]
Isoprene	Cholesterol synthesis, oxidative stress, metabolic conditions	Marker for lipid metabolism	[62]

Breath Gas (Biomarker)	Associated Disease / Condition	Diagnostic Role	Ref.
Ethanol	Liver disease, alcohol metabolism	Can be endogenous or due to alcohol consumption	[63]

5. Conclusion

In summary, Mg doped ZnO thin films were deposited on glass substrates using spray pyrolysis technique. Structural and optical properties of the ZnO thin films for three different Mg doping levels were investigated. At 2% Mg doping, the XRD pattern shows broader peaks which indicates smaller crystallite sizes and higher lattice strain. The films exhibit high optical transmittance, with the maximum value of nearly 90% observed for 2% Mg concentration and maintaining comparatively good transmittance values for higher Mg concentrations. The variation in the band gap (Eg) may be attributed to changes in crystallite size and strain in ZnO films. Morphologically, FESEM analysis reveals that 2% Mg result in compact grains with a higher surface area which promotes better gas diffusion and enhances gas sensing performance. For 2% Mg, the films show the highest gas sensor response (88%) with the fastest response and recovery times. These findings are particularly relevant for the detection of highly volatile gases such as acetone, which plays a crucial role as a biomarker in medical diagnostics and as a pollutant in industrial settings. The ability to detect low level acetone efficiently at room temperature further underscores the practical applicability of Mg doped ZnO films in low-power, non invasive and portable sensing devices.

Acknowledgment

The authors gratefully acknowledge the Department of Science and Technology (DST), Government of India, for the instrumental support provided under the DST-FIST Program to the Department of Physics, Dayanand Science College, Latur.

Authors Contribution

MBA- Characterization, Analysis, **LHK-** Methodology, **VSC-** Final drafting, **SDL-** Synthesis, Writing & Review.

Ethics declarations

Conflict of interest: The authors have no competing interests to declare that are relevant to the content of this article. The authors declare that they have no known competing financial interests or personal relationships that could have appeared to influence the work reported in this paper**.**

Data available on request from the authors

The data that support the findings of this study are not openly available due to reasons of sensitivity and are available from the corresponding author upon reasonable.

References

[1]Liu, H., Liu, W., Sun, C., Huang, W., & Cui, X. (2024). *A review of non-invasive blood glucose monitoring through breath acetone and body surface*. Sensors and Actuators A: Physical, 374, Article 115500. https://doi.org/10.1016/j.sna.2024.115500

[2]Murugesan, M., & Meher, S. R. (2024). *TiO_2–ZnO composite thin films fabricated by sol-gel spin coating for room-temperature impedometric acetone sensing*. Sensors and Actuators A: Physical, 369, Article 115181. https://doi.org/10.1016/j.sna.2024.115181

[3]Gupta, S., & Tai, N.-H. (2023). *Carbon nanomaterials and their composites for electrochemical glucose biosensors: A review on fabrication and sensing properties*. Journal of the Taiwan Institute of Chemical Engineers, 154, Article 104957. https://doi.org/10.1016/j.jtice.2023.104957

[4]Hilal, M., Ali, Y., Cai, Z., Kim, H., Abdo, H. S., Alnaser, I. A., & Hwang, Y. (2025). *3D flower-like Co_3O_4@ZnO nanostructures for trace-level acetone detection at low operating temperatures*. Sensors and Actuators A: Physical, 388, Article 116479. https://doi.org/10.1016/j.sna.2025.116479

[5]Panda, Sagarika and Mehlawat, Savita and Dhariwal, Neeraj and Kumar, Ashwani and Sanger, Amit. Comprehensive review on gas sensors: Unveiling recent developments and addressing challenges. Materials Science and Engineering: B, 308, (2024), 117616. http://dx.doi.org/10.1016/j.mseb.2024.117616

[6]Dussan, K., Hoek, M., de Vrije, T., van de Vondervoort, R., Bonouvrie, P., Caliskan, R., Parenti, A., Zegada-Lizarazu, W., Monti, A., Smit, A. T., & López-Contreras, A. M. (2025). *Performance of mild acetone organosolv fractionation on lignocellulosic feedstocks from new cropping systems for production of advanced bioethanol*.

Industrial Crops and Products, 223, Article 120156. https://doi.org/10.1016/j.indcrop.2024.120156

[7]Tarango Brito, E. C., Barrera Díaz, C. E., Ávila Córdoba, L. I., Frontana Uribe, B. A., & Solís Casados, D. A. (2025). *Recovery and Reuse of Acetone from Pharmaceutical Industry Waste by Solar Distillation*. Processes, 13(2), Article 361. https://doi.org/10.3390/pr13020361

[8]Natarajamani, Gowri Shonali and Kannan, Veera Prabu and Madanagurusamy, Sridharan. Synergistically enhanced NH_3 gas sensing of graphene oxide-decorated Nano-ZnO thin films. Materials Chemistry and Physics, 316, (2024), 129036. http://dx.doi.org/10.1016/j.matchemphys.2024.129036

[9]Sun, Guopan and Sun, Shanfu and Wang, Yinglin and Hao, Xidong and Hao, Yue and Liu, Chao and Gong, Caili and Yang, Qianyong and Du, Weian and Cheng, Pengfei. A novel gas sensor based on ZnO nanoparticles self-assembly porous networks for morphine drug detection in methanol. Sensors and Actuators B: Chemical, 420, (2024), 136495. http://dx.doi.org/10.1016/j.snb.2024.136495

[10]Maier, Christian and Leitgeb, Verena and Egger, Larissa and Köck, Anton. Size-Dependent Thresholds in CuO Nanowires: Investigation of Growth from Microstructured Thin Films for Gas Sensing. Nanomaterials, 14, (2024), 1207. http://dx.doi.org/10.3390/nano14141207

[11]El Filali, B. and Torchynska, T. and Ballardo Rodríguez, I. Ch. and Douda, J. and Polupan, G. Transmittance, structure and resistivity of ZnO films doped with Ga and In elements for TCO applications. Journal of Materials Science: Materials in Electronics, 34, (2023). http://dx.doi.org/10.1007/s10854-023-10313-0

[12]Liu, Maosheng and Jiang, Mingming and Zhao, Qinzhi and Tang, Kai and Sha, Shulin and Li, Binghui and Kan, Caixia and Shi, Da Ning. Ultraviolet Exciton-Polariton Light-

Emitting Diode in a ZnO Microwire Homojunction. ACS Applied Materials & Interfaces, 15, (2023), 13258-13269. http://dx.doi.org/10.1021/acsami.2c19806

[13]Sun, Kai and Zhan, Guanghui and Zhang, Lin and Wang, Zilin and Lin, Shiwei. Highly sensitive NO_2 gas sensor based on ZnO nanoarray modulated by oxygen vacancy with Ce doping. Sensors and Actuators B: Chemical, 379, (2023), 133294. http://dx.doi.org/10.1016/j.snb.2023.133294

[14]Prasad, Shital and Bansal, Sonia and Mansoori, Amir and Bala, Manju and Sharma, Preeti. Effect of Annealing Temperature on Excitonic Binding Energy and Other Optical Properties of Mn-Ni Co-Doped Transparent ZnO Thin Films. Transactions of the Indian Ceramic Society, 82, (2023), 31-39. http://dx.doi.org/10.1080/0371750x.2022.2160376

[15]Ponja, Sapna D. and Sathasivam, Sanjayan and Parkin, Ivan P. and Carmalt, Claire J. Highly conductive and transparent gallium doped zinc oxide thin films via chemical vapor deposition. Scientific Reports, 10, (2020). http://dx.doi.org/10.1038/s41598-020-57532-7

[16]M.A.M. Ahmed, W.E. Meyer, J.M. Nel Effect of (Ce, Al) co-doped ZnO thin films on the Schottky diode properties fabricated using the sol-gel spin coating, Materials Science in Semiconductor Processing, 103, (2019), 104612. http://dx.doi.org/10.1016/j.mssp.2019.104612.

[17]Bartholazzi, Gabriel and Pereira, Robson Pacheco and Lima, Andreza Menezes and Pinheiro, Wagner Anacleto and Cruz, Leila Rosa. Influence of substrate temperature on the chemical, microstructural and optical properties of spray deposited $CH_3NH_3PbI_3$ perovskite thin films. Journal of Materials Research and Technology, 9, (2020), 3411-3417. http://dx.doi.org/10.1016/j.jmrt.2020.01.078

[18]Sabhya and Kompa, Akshayakumar and Kekuda, Dhananjaya and Murari, M.S. and Mohan Rao, K. Influence of Hf precursor concentration on various properties of sol-

gel based spin coated HfO_2 thin films. Optical Materials, 136, (2023), 113424. http://dx.doi.org/10.1016/j.optmat.2022.113424

[19]Zhang, Can and Ding, Wanyu and Wang, Hualin And Chai, Weiping And Ju, Dongying. Influences of working pressure on properties for TiO_2 films deposited by DC pulse magnetron sputtering. Journal of Environmental Sciences, 21, (2009), 741-744. http://dx.doi.org/10.1016/s1001-0742(08)62334-7

[20]Chen Y, Liu Y, Liu J, Li Y, Liu Y, Zhang W, Han L, Wang D, Cao S, Liu H, Xie Q, Wang X, Zhang M, 2024. Porous PDMS–ZnO wearable gas sensor for acetone biomarker detection and breath analysis. *ACS Applied Materials & Interfaces*, 16(45), 62436–62445. https://doi.org/10.1021/acsami.4c16209

[21]Kumar S, Bhowmik B, 2024. Frequency-tuned selectivity enhancement of Mg@ZnO–TiO_2 nanoflake-based heterojunction sensor devices. *Analyst*, 149, 1895–1906. https://doi.org/10.1039/D3AN01562A

[22]Prabhu NN, Shivamurthy B, Anandhan S, et al., 2024. Effect of Ni doping on the acetone vapor sensing performance of ZnO nanofibers. *Ceramics International*. https://doi.org/10.1016/j.ceramint.2024.11.055

[23]Jaballah S, Alaskar Y, AlShunaifi I, Ghiloufi I, Neri G, Bouzidi C, Dahman H, El Mir L, 2021. Effect of Al and Mg doping on reducing gases detection of ZnO nanoparticles. *Chemosensors*, 9(11), 300. https://doi.org/10.3390/chemosensors9110300

[24]Parveen RA, Vinoth E, Hara K, Archana J, Ponnusamy S, Navaneethan M, 2024. Synergistic tailoring of adsorption and vacancy enrichment in lamellar-stacked α-MoO_3 nanorods by Mg^{2+} for a NO_2 gas sensor. *Sensors and Actuators B: Chemical*, 417, 136017. https://doi.org/10.1016/j.snb.2024.136017

[25]Kang, Yanli and Yu, Feng and Zhang, Lu and Wang, Wenhao and Chen, Long and Li, Yingchun. Review of ZnO-based nanomaterials in gas sensors. Solid State Ionics, 360, (2021), 115544. http://dx.doi.org/10.1016/j.ssi.2020.115544

[26]Liang, Yuan-Chang and Zhao, Wei-Cheng. Morphology-dependent photocatalytic and gas-sensing functions of three-dimensional TiO_2-ZnO nanoarchitectures. CrystEngComm, 22, (2020), 7575-7589. http://dx.doi.org/10.1039/d0ce01036g

[27]Mani, Dinesh and Sundar Manoharan, S. and Johnsy Arputhavalli, G. and Sriram, Ganesan and Jebasingh, S. A study on morphology dependent nanostructured ZnO thin films: An efficient gas sensing response for acetaldehyde. Inorganic Chemistry Communications, 150, (2023), 110471. http://dx.doi.org/10.1016/j.inoche.2023.110471

[28]Bendahmane, B., Tomić, M., Touidjen, N. E. H., Gràcia, I., Vallejos, S., & Mansour, F. (2020). *Influence of Mg doping levels on the sensing properties of SnO_2 films*. Sensors, *20*(7), Article 2158. https://doi.org/10.3390/s20072158

[29]Kara, R., Mentar, L., & Azizi, A. (2020). *Synthesis and characterization of Mg-doped ZnO thin-films electrochemically grown on FTO substrates for optoelectronic applications*. RSC Advances, *10*, 40467–40475. https://doi.org/10.1039/d0ra06541b

[30]Wei, X., Yang, X., Guo, Y., Liu, Y., Wang, L., Wang, Q., Cheng, L., & Jiao, Z. (2024). *UV-enhanced Mg:MOF-ZnO sensor for n-butanol gas detection at a lower operating temperature*. Applied Surface Science, *678*, Article 161138. https://doi.org/10.1016/j.apsusc.2024.161138

[31]Kaim, Paulina and Lukaszkowicz, Krzysztof and Szindler, Marek and Szindler, Magdalena M. and Basiaga, Marcin and Hajduk, Barbara. The Influence of Magnetron Sputtering Process Temperature on ZnO Thin-Film Properties. Coatings, 11, (2021), 1507. http://dx.doi.org/10.3390/coatings11121507

[32]Gerbreders, Vjaceslavs and Krasovska, Marina and Sledevskis, Eriks and Gerbreders, Andrejs and Mihailova, Irena and Tamanis, Edmunds and Ogurcovs, Andrejs. Hydrothermal synthesis of ZnO nanostructures with controllable morphology change. CrystEngComm, 22, (2020), 1346-1358. http://dx.doi.org/10.1039/c9ce01556f

[33]Khan, M.I. and Bhatti, K.A. and Qindeel, Rabia and Alonizan, Norah and Althobaiti, Hayat Saeed. Characterizations of multilayer ZnO thin films deposited by sol-gel spin coating technique. Results in Physics, 7, (2017), 651-655. http://dx.doi.org/10.1016/j.rinp.2016.12.029

[34]Patil, Vithoba L. and Vanalakar, Sharadrao A. and Patil, Pramod S. and Kim, Jin H.. Fabrication of nanostructured ZnO thin films based NO_2 gas sensor via SILAR technique. Sensors and Actuators B: Chemical, 239, (2017), 1185-1193. http://dx.doi.org/10.1016/j.snb.2016.08.130

[35]Sener, Emre and Bayram, Ozkan and Hasar, Ugur Cem and Simsek, Onder. Structural and optical properties of RF sputtered ZnO thin films: Annealing effect. Physica B: Condensed Matter, 605, (2021), 412421. http://dx.doi.org/10.1016/j.physb.2020.412421

[36]Hambi, M. and Khadraoui, M. and Miloua, R. and Bouzidi, A. and Nakrela, A. and Medles, M. and Amara, Z.. Structural evolution and photocatalytic performance of ZnS–ZnO thin films synthesized by spray pyrolysis. Ceramics International, 50, (2024), 35902-35914. http://dx.doi.org/10.1016/j.ceramint.2024.07.081

[37]Awale, M.*, Lokhande, S. D.*, Kadam, S. B., Mote, V. D., & Kadam, A. B. (2024). *Highly sensitive and selective room temperature acetone sensing properties of Co-doped ZnO nanostructure films*. Journal of Materials Science: Materials in Electronics, 35(18), Article 1209. https://doi.org/10.1007/s10854-024-12912-x

[38]Kumar, K. Naveen and Karkal, R. Naina and Shaik, Habibuddin and Jafri, R. Imran and Maligi, Anantha Sunil and Salimath, S. Darshan and Singh, Omkar and Ramya, H. G. Deposition and characterization of ZnO thin films on corning glass substrate using Magnetron sputtering. AIP Conference Proceedings, 3122, (2024), 050001. http://dx.doi.org/10.1063/5.0215977

[39]Anitha, M. and Tamilnayagam, V. and Anitha, N. and Devendhiran, Tamiloli and Kumarasamy, Keerthika and Thangaraj, Vasudevan and Devendhiran, Kannagi and Amalraj, L.. Influence of Carrier Gas Pressure on the Physical Properties of CdO Thin Films. Zeitschrift für Physikalische Chemie, 233, (2018), 913-932. http://dx.doi.org/10.1515/zpch-2018-1227

[40]Hameed, S. Sahul and Balayazhini, B. and Amalraj, L. and Zahirullah, S. Syed and Mohamed, J. Raj. Impact of carrier gas pressures in the formation of (103) oriented In_2S_3 nanocrystalline thin films by Nebulized Spray Pyrolysis method. Journal of Materials Science: Materials in Electronics, 34, (2023). http://dx.doi.org/10.1007/s10854-022-09413-0

[41]Petlacalco Ramírez, Héctor Eduardo and Alcántara Iniesta, Salvador and Soto Cruz, Blanca Susana and Mejía Silva, Jesús Israel. Evaluation of the Piezoresistivity of a Thin Film of ZnO Doped with Fluorine and Deposited via the Ultrasonic Spray Pyrolysis Technique for Applications in Micro/Nano-Electromechanical Sensors. Crystals, 12, (2022), 1607. http://dx.doi.org/10.3390/cryst12111607

[42]Arulanantham, A M S and Valanarasu, S and Jeyadheepan, K and Kathalingam, A. Effect of carrier gas pressure on structural, optical and photovoltaic properties of tin sulphide thin films prepared by nebulizer spray pyrolysis method. Bulletin of Materials Science, 42, (2019). http://dx.doi.org/10.1007/s12034-019-1772-x

[43]Mishra, Sushma and Przezdziecka, Ewa and Wozniak, Wojciech and Adhikari, Abinash and Jakiela, Rafal and Paszkowicz, Wojciech and Sulich, Adrian and Ozga, Monika and Kopalko, Krzysztof and Guziewicz, Elzbieta. Structural Properties of Thin ZnO Films Deposited by ALD under O-Rich and Zn-Rich Growth Conditions and Their Relationship with Electrical Parameters. Materials, 14, (2021), 4048. http://dx.doi.org/10.3390/ma14144048

[44]Waseem, Salma and Anjum, Safia and Zeeshan, Talat and Shah, Ismat. Effects of Cr-doping on structural, morphological, magnetic, optical and electrical properties of $Ti_{0.9}Fe_{0.1-x}O_2$ thin films. Optik, 212, (2020), 164630. http://dx.doi.org/10.1016/j.ijleo.2020.164630

[45]Habibi, Ali and Vatandoust, Leila and Aref, Sajedeh Mohammadi and Naghshara, Hamid. Formation of high performance nanostructured ZnO thin films as a function of annealing temperature: structural and optical properties. Surfaces and Interfaces, 21, (2020), 100723. http://dx.doi.org/10.1016/j.surfin.2020.100723

[46]Mariappan, R. and Ponnuswamy, V. and Suresh, P.. Effect of doping concentration on the structural and optical properties of pure and tin doped zinc oxide thin films by nebulizer spray pyrolysis (NSP) technique. Superlattices and Microstructures, 52, (2012), 500-513. http://dx.doi.org/10.1016/j.spmi.2012.05.016

[47]Hassanien, Ahmed Saeed and Akl, Alaa A. Optical characteristics of iron oxide thin films prepared by spray pyrolysis technique at different substrate temperatures. Applied Physics A, 124, (2018). http://dx.doi.org/10.1007/s00339-018-2180-6

[48]Abdel-Galil, A. and Hussien, Mai S.A. and Yahia, I.S. Synthesis and optical analysis of nanostructured F-doped ZnO thin films by spray pyrolysis: Transparent electrode for photocatalytic applications. Optical Materials, 114, (2021), 110894. http://dx.doi.org/10.1016/j.optmat.2021.110894

[49]Farhadian Azizi, K. and Bagheri- Mohagheghi, M.- M. The effect of solution flow rate and substrate temperature on structural and optical properties of TiO_2 films deposited by spray pyrolysis technique. Thin Solid Films, 621, (2017), 98-101. http://dx.doi.org/10.1016/j.tsf.2016.11.040

[50]Ennaceri, Houda and Boujnah, Mourad and Erfurt, Darja and Rappich, Jörg and Lifei, Xi and Khaldoun, Asmae and Benyoussef, Abdelilah and Ennaoui, Ahmed and Taleb, Abdelhafed. Influence of stress on the photocatalytic properties of sprayed ZnO thin

films. Solar Energy Materials and Solar Cells, 201, (2019), 110058. http://dx.doi.org/10.1016/j.solmat.2019.110058

[51]Eslamian, Morteza and Ashgriz, Nasser. Effect of precursor, ambient pressure, and temperature on the morphology, crystallinity, and decomposition of powders prepared by spray pyrolysis and drying. Powder Technology, 167, (2006), 149-159. http://dx.doi.org/10.1016/j.powtec.2006.06.016

[52]Deshmukh, S.B. and Bari, R.H. Nanostructured ZrO Thin Films Deposited by Spray Pyrolysis Techniques for Ammonia Gas Sensing Application. International Letters of Chemistry, Physics and Astronomy, 56, (2015), 120-130. http://dx.doi.org/10.56431/p-ol42l6

[53]Tischner, Alexandra and Maier, Thomas and Stepper, Christoph and Köck, Anton. Ultrathin SnO_2 gas sensors fabricated by spray pyrolysis for the detection of humidity and carbon monoxide. Sensors and Actuators B: Chemical, 134, (2008), 796-802. http://dx.doi.org/10.1016/j.snb.2008.06.032

[54]Hastir, Anita and Kohli, Nipin and Singh, Ravi Chand. Temperature dependent selective and sensitive terbium doped ZnO nanostructures. Sensors and Actuators B: Chemical, 231, (2016), 110-119. http://dx.doi.org/10.1016/j.snb.2016.03.001

[55]Chu, Yen-Lin and Ji, Liang-Wen and Xie, Jun-Hong and Chu, Tung-Te. High-Sensitivity of Self-Powered Gas Sensors Based on Piezoelectric Nanogenerators With Y-Doped 1-D ZnO Nanostructures. IEEE Sensors Journal, 24, (2024), 18731-18739. http://dx.doi.org/10.1109/jsen.2024.3389931 .

[56] Usman, F.; Ghazali, K. H.; Muda, R.; Dennis, J. O.; Ibnaouf, K. H.; Aldaghri, O. A.; Alsadig, A.; Johari, N. H.; Jose, R. Detection of kidney complications relevant concentrations of ammonia gas using plasmonic biosensors: a review. Chemosensors, 11 (2023), 119. http://dx.doi.org/10.3390/chemosensors11020119

[57]Konstantinidi, E. M.; Lappas, A. S.; Tzortzi, A. S.; Behrakis, P. K. Exhaled breath condensate: technical and diagnostic aspects. The Scientific World Journal, 2015 (2015), 435160. http://dx.doi.org/10.1155/2015/435160

[58] Osborne, J.; Sobh, M.; Trudel, G. Carbon monoxide as a clinical marker of hemolysis. American Journal of Hematology, 98(7) (2023). http://dx.doi.org/10.100 2/ajh.26958

[59]Viana, K. S. S.; Eleutério, F. H. P. F.; Maciel, V. G.; Bernis, C. S.; Souza, A. C. M.; Lima, R. P. E.; Cota, L. O. M.; et al. Association between halitosis and gastrointestinal disorders: a review. Journal of the California Dental Association, (2024). http://dx.doi.org/10.1080/19424396.2024.2426249 .

[60]Gandhi, M.; et al. Methane-positive small intestinal bacterial overgrowth in inflammatory bowel disease and irritable bowel syndrome: a systematic review and meta-analysis. Gut Microbes, 13 (2021), 1933313. http://dx.doi.org/10.1080/19490976.2021.1933313 .

[61]Turner C, Walton C, Hoashi S, Evans M, 2009. Breath acetone concentration decreases with blood glucose concentration in type 1 diabetes mellitus. *Journal of Breath Research*, 3(4), 046004. https://doi.org/10.1088/1752-7155/3/4/046004

[62]Massey, B. T.; Wald, A. Small intestinal bacterial overgrowth syndrome: a guide for the appropriate use of breath testing. Digestive Diseases and Sciences, 66(2) (2021), 338–347. http://dx.doi.org/10.1007/s10620-020-06623-6 .

[63]Mojumder, S.; Das, T.; Das, S.; Chakraborty, N.; Saha, D.; Pal, M. Y- and Al-co-doped ZnO nanopowder-based ultrasensitive trace ethanol sensor: a potential breath analyzer for fatty liver disease and drunken-driving detection. Sensors and Actuators B: Chemical, 372 (2022), 132611. http://dx.doi.org/10.1016/j.snb.2022.132611.